Second Harmonic Generation Spectroscopy in the Reststrahl Band of SiC Using an Infrared Free-Electron Laser

Alexander Paarmann,[a] Ilya Razdolski, Alexey Melnikov, Sandy Gewinner, Wieland Schöllkopf, and Martin Wolf
Fritz-Haber-Institut der Max-Planck-Gesellschaft, Faradayweg 4-6, 14195 Berlin, Germany

(Dated: September 8, 2015)

The Reststrahl spectral region of Silicon Carbide has recently attracted much attention owing to its potential for mid-infrared nanophotonic applications based on surface phonon polaritons (SPhPs). Studies of optical phonon resonances responsible for surface polariton formation, however, have so far been limited to linear optics. In this Letter, we report the first nonlinear optical investigation of the Reststrahl region of SiC, employing an infrared free-electron laser to perform second harmonic generation (SHG) spectroscopy. We observe two distinct resonance features in the SHG spectra, one attributed to resonant enhancement of the nonlinear susceptibility $\chi^{(2)}$ and the other due to a resonance in the Fresnel transmission. Our work clearly demonstrates high sensitivity of mid-infrared SHG to phonon-driven phenomena, and opens a route to studying nonlinear effects in nanophotonic structures based on SPhPs.

PACS numbers: 78.47.N-,78.30.-j,63.20.-e
Keywords: Reststrahl, Second Harmonic, Phonons, Silicon Carbide

In recent years, there has been considerable interest in the mid-infrared *Reststrahl*[1] spectral region of Silicon Carbide (SiC),[2–6] since it holds much promise for a novel approach to low-loss, mid-infrared (IR) nanophotonic applications based on surface phonon polaritons (SPhPs).[4,5] Similarly to surface plasmon polaritons in metals, these surface phonon waves in the Reststrahl band of polar dielectrics can be tailored using resonant optical nano-antennas[4,5] as the fundamental building block of future nanophotonic devices.[7,8] Most importantly, nanophotonics based on SPhPs could solve the intrinsic optical loss-problem of plasmonics,[9] making use of the much smaller damping rates of phonons as compared to plasmons.[6]

The peculiar linear optical properties in the Reststrahl region responsible for SPhP formation are dominated by dielectric response of the optical phonons in polar dielectrics.[10] The polar bonding character leads to splitting of the transversal optical (TO) and longitudinal optical (LO) phonon branches at the Brillouin zone-center and IR activity of the zone-center TO phonon. As a result, the TO phonon appears as a sharp resonance in the dielectric function $\varepsilon(\omega) = \varepsilon_1 + i\varepsilon_2$, accompanied with a zero-crossing of ε_1 at the zone-center TO frequency ω_{TO}, whereas the macroscopic polarization associated with LO modes produces the second zero-crossing of ε_1 at ω_{LO}.[10] Therefore, ε_1 is negative between TO and LO phonon frequencies constituting the bulk phonon polariton gap where only SPhPs can exist, defining the Reststrahl band of near-perfect reflectivity.[1,10]

In order to improve the engineering of future nanophotonic devices based on SPhPs, exact knowledge of the dielectric response in the Reststrahl region is desired. However, linear optical techniques like reflectivity only provide indirect information, and require differentiation to extract the resonances.[11,12] As one possible solution, nonlinear optical spectroscopy could provide improved sensitivity to critical features in the dielectric response.[13,14] Such studies have been hindered by the sparsity of intense and narrowband laser sources in the mid-IR frequency range and low nonlinear signal levels, such that only few nonlinear optical experiments in the Reststrahl region appear in the literature[15–18] with no reports for SiC.

In this Letter, we use narrowband, intense mid-IR pulses generated from a free-electron laser (FEL)[19] to perform the first spectroscopic study of second harmonic generation (SHG) in the Reststrahl region of 4H-SiC. We observe two distinct spectral features in the SHG response, one at the TO frequency resulting from the resonance in the nonlinear susceptibility $\chi^{(2)}$, and another one in the LO frequency range due to resonant enhancement of the Fresnel transmission. Theoretical modeling of the SHG spectra reveals the details of the underlying mechanisms, showing that mid-IR SHG is very sensitive to the critical features of the linear and nonlinear optical response in the Reststrahl band.

The experimental setup resembles a typical non-collinear autocorrelator and is schematically shown in Fig. 1 (a). The incoming FEL beam is split into two equal parts and focused on the sample at incidence angles of $\sim 62°$ and $\sim 28°$, respectively. The optical delay between both autocorrelator arms can be adjusted using a motorized translation stage. At zero delay, two-pulse correlated second harmonic (SH) radiation is generated in reflection, spatially centered between the reflected fundamental beams. The SHG signal is spatially filtered, and detected with a liquid nitrogen cooled mercury cadmium telluride/indium antimony sandwich detector (Infrared Associates).

[a] Electronic mail: alexander.paarmann@fhi-berlin.mpg.de

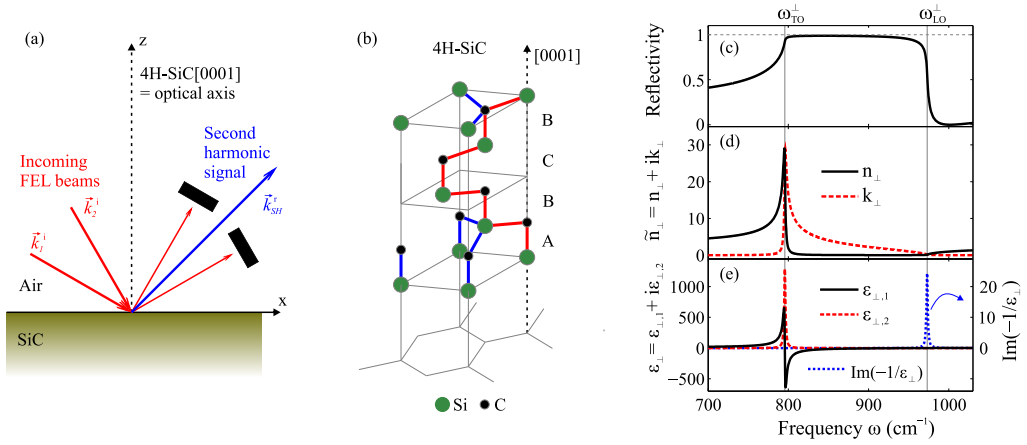

Figure 1. (a) Schematic of the SHG spectroscopy experiment. (b) Schematic crystal structure of 4H-SiC, also indictating the stacking sequence. (c) Reflectivity in the Reststrahl band, calculated for (d) the complex refractive index and (e) dielectric function of ordinary rays in 4H-SiC.[20] Also shown in (e) is the quantity $\mathrm{Im}(-1/\varepsilon_\perp)$ that peaks at the zero-crossing of $\varepsilon_{\perp,1}$ (blue-dotted line).

Details on the FEL are given elsewhere.[19] In short, the electron accelerator is operated at a micropulse repetition rate of 1 GHz with electron macropulse duration of 10 μs at macropulse repetition rate of 10 Hz. The electron energy is set to 26.5 MeV, and the FEL output can be tuned between $450-1150$ cm^{-1} using the motorized undulator gap, with typical spectral bandwidth of $\sim$5 cm^{-1} and micropulse energies of up to $\sim$10 μJ. The FEL beam is intrinsically p-polarized; polarization rotation to s-pol for one or both beams is realized by two subsequent wire-grid polarizers (Thorlabs), set to 45 and 90 deg with respect to the incoming polarization, respectively.

The sample investigated here is a semi-insulating z-cut single crystal of 4H-SiC, i.e., with the c-axis of the hexagonal crystal structure perpendicular to the sample surface, see Fig. 1 (b). The optical axis of this birefringent SiC polytype coincides with the c-axis, resulting in extraordinary and ordinary ray propagation for p-pol and s-pol fundamental beams, respectively. The dispersion of the reflectivity, refractive index, and dielectric function for ordinary rays of 4H-SiC, calculated using a classical dispersion model,[20] is shown in Fig. 1 (c-e), illustrating how the optical phonon resonances lead to the Reststrahl effect. Additionally, we plot the quantity $\mathrm{Im}\,(-1/\varepsilon)$ in Fig. 1 (e), since it conveniently peaks at the zero-crossing of ε_1 at the LO frequency.[10]

The general theory of SHG is well established.[13] Here,We focus here on resonant mid-IR SHG in reflection with non-collinear two-pulse excitation, see Fig. 1 (a). Two tunable IR beams of frequency ω with incoming wave vectors $\vec{k}_1^i$ and $\vec{k}_2^i$ at angles of incidence θ_1^i and θ_2^i, respectively, impinge on the sample. SH radiation is generated in reflection at frequency 2ω at an angle $\theta_{SH}^r = \arcsin\left[\left(\sin\theta_1^i + \sin\theta_2^i\right)/2\right] \approx (\theta_1^i + \theta_2^i)/2$. For crystals lacking inversion symmetry, the surface contribution to the second-order nonlinear signals is typically negligible.[13] We here consider the bulk SH polarization of the form

$$\vec{P}(2\omega) \propto \overleftrightarrow{\chi}^{(2)}(2\omega,\omega,\omega) : (\overleftrightarrow{L}_1(\omega)\vec{E}_1(\omega))(\overleftrightarrow{L}_2(\omega)\vec{E}_2(\omega)), \tag{1}$$

where $\overleftrightarrow{L}_{1(2)}$ are the Fresnel transmission tensors for the two incident beams representing the macroscopic local field corrections,[13] and $\vec{E}_{1(2)}$ are the incident electric field vectors. The reflected second harmonic intensity is given by projecting the nonlinear polarization onto the field direction of the reflected SH beam.[13]

In the following, we consider laboratory frame coordinates (x, y, z), with the z-axis parallel to the surface normal and the c-axis of hexagonal SiC, and the x-z plane defining the plane of incidence, see Fig. 1 (a). For the uniaxial 4H-SiC crystal, the birefringence must be treated explicitly,[21] resulting in the following non-vanishing components of the Fresnel transmission tensor:

$$\begin{aligned} L_{xx}(\theta^i,\omega) &= \frac{2k_{z,e}^t(\theta^i,\omega)}{\varepsilon_\perp(\omega)k_z^i(\theta^i,\omega) + k_{z,e}^t(\theta^i,\omega)} \\ L_{yy}(\theta^i,\omega) &= \frac{2k_z^i(\theta^i,\omega)}{k_z^i(\theta^i,\omega) + k_{z,o}^t(\theta^i,\omega)} \\ L_{zz}(\theta^i,\omega) &= \frac{\varepsilon_\perp(\omega)}{\varepsilon_\parallel(\omega)} \frac{2k_z^i(\theta^i,\omega)}{\varepsilon_\perp(\omega)k_z^i(\theta^i,\omega) + k_{z,e}^t(\theta^i,\omega)} \end{aligned} \tag{2}$$

with $\varepsilon_{xx} = \varepsilon_{yy} = \varepsilon_\perp(\omega)$ and $\varepsilon_{zz} = \varepsilon_\parallel(\omega)$ being the elements of the diagonal dielectric tensor, and $k_{z,o(e)}^t(\omega)$ the z-component of the complex wave vectors of the transmitted fundamental ordinary (extraordinary) waves inside the medium.[21] 4H-SiC has hexagonal structure of point-group symmetry $6mm$, leading to the following non-vanishing components of the second-order susceptibility for SHG:[22]

$$\chi_{zzz}^{(2)},\ \chi_{zxx}^{(2)} = \chi_{zyy}^{(2)},\ \chi_{xzx}^{(2)} = \chi_{yzy}^{(2)} = \chi_{xxz}^{(2)} = \chi_{yyz}^{(2)}. \tag{3}$$

In consequence, we expect non-zero SHG signals from four different measurements with polarization combinations denoted as PSS (p-polarized SHG, s-polarized fundamental beams 1 and 2, respectively), PPP, SPS, and SSP. Here, we consider the PSS and SPS geometries only since they each contain a single $\chi^{(2)}$ tensor component; their SH intensities have the following form:[13]

$$I_{PSS}(2\omega) \propto \Big| \sin(\theta^r_{SH})\chi^{(2)}_{zyy}(2\omega,\omega,\omega) \times \times L_{yy}(\omega,\theta^i_1)L_{yy}(\omega,\theta^i_2)\Big|^2/\Delta k^2_{PSS}$$

$$I_{SPS}(2\omega) \propto \Big| \chi^{(2)}_{yzy}(2\omega,\omega,\omega) \times \times \sin(\theta^i_1)L_{zz}(\omega,\theta^i_1)L_{yy}(\omega,\theta^i_2)\Big|^2/\Delta k^2_{SPS} \quad (4)$$

where $\Delta k = |\vec{k}^t_{SH} - \vec{k}^t_1 - \vec{k}^t_2|$ accounts for the wave vector mismatch in reflection. We neglect the Fresnel factors $L(2\omega,\theta^r_{SH})$ for the SH transmission from the crystal into air[13,18] since these are dispersionless at SH frequencies.

For a detailed analysis of the experimental SHG spectra, line shape models for ε and $\chi^{(2)}$ near the optical phonon resonances are needed. For $\chi^{(2)}$, Flytzanis[23] considered three different contributions containing linear, 2nd, and 3rd order terms of TO phonon resonances, which are usually denoted Faust-Henry,[24] electrical and mechanical anharmonicity,[23,25] respectively. In consequence, the $\chi^{(2)}$ tensor is expected to be anisotropic, since the planar and axial phonon frequencies for polarization perpendicular and along the c-axis direction, respectively, are different.[12,26] Employing a classical dielectric function model[20] with anisotropic phonon frequencies, the SHG signals for 4H-SiC can be calculated using Eq. 4. Finally, variation of the phonon frequencies and $\chi^{(2)}$ lineshape parameters allows fitting of this model to the experimental data.

The experimental SHG spectra of 4H-SiC for the PSS and SPS geometries are shown in Fig. 2, as well as fits to the data using Eq. 4 and the line shape model for the second-order susceptibility.[25] For all spectra, there are two distinct regions of interest: around the TO resonance at 797 cm^{-1}, region (i), and around the LO resonances in the range of 950-1000 cm^{-1}, region (ii), highlighted in green and blue in Fig. 2, respectively. We first focus on region (i): resonant enhancement of SHG at the TO frequency is well expected since zone-center TO phonons are the only optical resonances in this frequency region, and should lead to a sharp enhancement of $\chi^{(2)}$.[25] Notably, we only observe enhanced SHG yield at the planar TO frequency $\omega^{\perp}_{TO}$, while any possible resonance at the axial TO frequency $\omega^{\parallel}_{TO}$ is suppressed. From our model, even the resonance at $\omega^{\perp}_{TO}$ is suppressed for the SPS geometry, and the small remnant SHG signal observable in region (i) likely originates from imperfect polarization states of the beams.

The large signals in region (ii) are surprising at first, since no $\chi^{(2)}$ resonance is expected for IR-inactive LO phonons. Still, we observe a very sharp and intense SHG peak at the axial LO phonon frequency $\omega^{\parallel}_{LO}$ for SPS, and a broader and blue-shifted resonance for PSS, see Fig. 2 (d) and (a), respectively.

The observations can be rationalized by inspection of the dispersion of the nonlinear susceptibility and the combined Fresnel factors from both fundamental beams plotted in Fig. 2 (b,e), that enter into the SHG signals, see Eq. 4. The $\chi^{(2)}$ line shape is dominated by a single resonance at $\omega^{\perp}_{TO}$ for PSS, and a double resonance at $\omega^{\perp}_{TO}$ and $\omega^{\parallel}_{TO}$ for SPS, reflecting the ordinary ray and mixed ordinary/extraordinary ray fundamental beams, respectively. In region (ii), the $\chi^{(2)}$ line shape is basically flat. The Fresnel factors shown in Fig. 2 (b,e) essentially behave inversely to the dielectric function, leading to an antiresonance at the TO frequencies in region (i) and a resonance at the LO frequencies, i.e., at the zero-crossings of $\varepsilon_{1,\perp}$ and $\varepsilon_{1,\parallel}$ in region (ii).

Remarkably, the TO phonon resonance in the dielectric response leads to very effective screening of the external fields and strong suppression of the macroscopic local fields in region (i) that, for SPS, completely compensates the pronounced resonance in $\chi^{(2)}$ in the total SHG yield. For PSS, this compensation is incomplete because of the higher order terms, i.e., electrical and mechanical anharmonicity,[23] in the line shape model of $\chi^{(2)}$. For region (ii) however, the flatness of $\chi^{(2)}$ makes the SHG yields extremely sensitive to the large local fields near zero-crossings of ε_1.

Moreover, the comparison of Fig. 1 (c) and Fig. 2 (a,d) shows that the peculiarities of linear optical properties (defining the Fresnel factors) at the edges of the Reststrahl region are much better accessible with the nonlinear-optical probe: the sharp and intense SHG peaks observed in Fig. 2 (a) and (d) possess much richer structure than the slopes of the reflectivity in Fig. 1 (c). Additionally, the different polarization conditions accessible with SHG allow detailed understanding of the anisotropic optical response. Therefore, mid-IR SHG spectroscopy manifests itself as a promising tool for studies and characterization of fundamental physical properties of bulk and nanophotonic Reststrahl materials, while the known low efficiency of the SHG process with respect to the linear-optical response is fully compensated by the high brilliance of the FEL.

In conclusion, we used an infrared free-electron laser to perform SHG spectroscopy of 4H-SiC in the Reststrahl region. We find two distinct resonant features in the response which we attribute, with the help of theoretical modeling, to resonances in the nonlinear susceptibility and in the Fresnel transmission at TO and LO phonon frequencies, respectively. Our data clearly demonstrates the great role of resonant behavior of the Fresnel factors in the enhancement of nonlinear-optical signal. The narrowband, widely tunable and intense FEL pulses are ideally suited for spectroscopic studies of mid-IR nonlinear optical response. In the future, the technique will be used to investigate the SHG response of nanophotonic systems based on SPhPs.

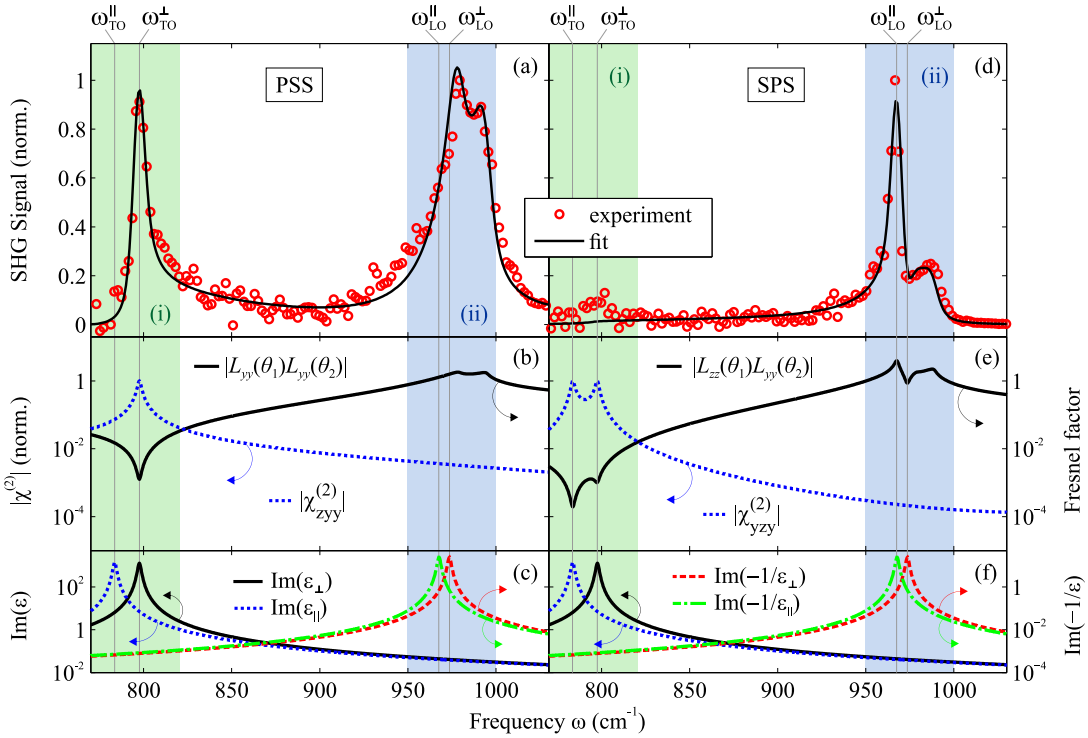

Figure 2. Experimental Reststrahl SHG spectra (red circles) of 4H-SiC for different polarization conditions: PSS (a) and SPS (d). Also shown are fits to the data (black full line), using Eq. 4 and the $\chi^{(2)}$ line shape model.[25] Two distinct resonance features are observed in the TO frequency region (i) (green shade) and LO frequency region (ii) (blue shade). To illustrate the origin of the resonant features, we show the dispersion of $\chi^{(2)}$ and the combined Fresnel transmission factors (b,e), as extracted from the fits to the data for each polarization condition. For reference, we additionally plot the dielectric function[20] and the quantity Im $(-1/\varepsilon)$ that peak at ω_{TO} and ω_{LO}, respectively,[10] for polarization parallel ($\|$) and perpendicular ($\perp$) to the c-axis (c,f). Please note the logarithmic scale used for (b,c,e,f).

The authors thank K. Horn and J.D. Caldwell for providing SiC samples, and M.B. Raschke for helpful discussions. A. M. gratefully acknowledges financial support by the Deutsche Forschungsgemeinschaft through project ME3570/1.

REFERENCES

[1] H. Rubens and F. Kurlbaum, Ann. Phys. **309**, 649 (1901).
[2] A. J. Huber, N. Ocelic, D. Kazantsev, and R. Hillenbrand, Appl. Phys. Lett. **87**, 081103 (2005).
[3] T. Taubner, D. Korobkin, Y. Urzhumov, G. Shvets, and R. Hillenbrand, Science **313**, 1595 (2006).
[4] J. D. Caldwell, O. J. Glembocki, Y. Francescato, N. Sharac, V. Giannini, F. J. Bezares, J. P. Long, J. C. Owrutsky, I. Vurgaftman, J. G. Tischler, V. D. Wheeler, N. D. Bassim, L. M. Shirey, R. Kasica, and S. A. Maier, Nano Lett. **13**, 3690 (2013).
[5] T. Wang, P. Li, B. Hauer, D. Chigrin, and T. Taubner, Nano Lett. , 5051 (2013).
[6] J. D. Caldwell, L. Lindsay, V. Giannini, I. Vurgaftman, T. L. Reinecke, S. A. Maier, and O. J. Glembocki, Nanophotonics **4**, 1 (2015).
[7] J. Anker, W. Hall, O. Lyandres, and N. Shah, Nat. Mater. **7**, 8 (2008).
[8] G. Konstantatos and E. H. Sargent, Nat. Nanotechnol. **5**, 391 (2010).
[9] J. B. Khurgin, Nat. Nanotechnol. **10**, 2 (2015).
[10] S. Adachi, *Opt. Prop. Cryst. Amorph. Semicond.* (Springer US, Boston, MA, 1999).
[11] K. Narita, Y. Hijikata, H. Yaguchi, S. Yoshida, and S. Nakashima, Jpn. J. Appl. Phys. **43**, 5151 (2004).
[12] H. Mutschke, A. Anderson D. Clement Th. Henning and G. Peiter, Astron. Astrophys. **345**, 187 (1999).
[13] Y. Shen, Annu. Rev. Phys. Chem. **40**, 327 (1989).
[14] S. Rashkeev, W. Lambrecht, and B. Segall, Phys. Rev. B **57**, 9705 (1998).
[15] A. Mayer and F. Keilmann, Phys. Rev. B **33** (1986).
[16] M. Barmentlo, G. W. t Hooft, E. R. Eliel, E. W. M. van der Ham, Q. H. F. Vrehen, A. F. G. van der Meer, and P. W. van Amersfoort, Phys. Rev. A **50**, R14 (1994).
[17] T. Dekorsy, V. Yakovlev, W. Seidel, M. Helm, and F. Keilmann, Phys. Rev. Lett. **90**, 055508 (2003).
[18] W.-T. Liu and Y. R. Shen, Phys. Rev. B **78**, 024302 (2008).
[19] W. Schöllkopf, S. Gewinner, H. Junkes, A. Paarmann, G. von Helden, H. Bluem, and A. M. M. Todd, Proc. SPIE **9512**, 95121L (2015).
[20] S. Nakashima and H. Harima, J. Appl. Phys. **95**, 3541 (2004).
[21] L. P. Mosteller, Jr. and F. Wooten, J. Opt. Soc. Am. **58**, 511 (1968).
[22] Y. R. Shen, *The Principles of Nonlinear Optics* (Wiley-Interscience, 2003).
[23] C. Flytzanis, Phys. Rev. B **6**, 1264 (1972).
[24] W. Faust and C. Henry, Phys. Rev. Lett. **17**, 1265 (1966).
[25] E. Roman, J. Yates, M. Veithen, D. Vanderbilt, and I. Souza, Phys. Rev. B **74**, 245204 (2006).
[26] H. Harima, S.-I. Nakashima, and T. Uemura, J. Appl. Phys. **78**, 1996 (1995).